Journal of Micromechanics and Microengineering

PAPER

Deep isotropic chemical etching (DICE) process for fabricating highly symmetric hemispherical silicon molds

To cite this article: Calvin Mitchell Jones *et al* 2021 *J. Micromech. Microeng.* **31** 075005

View the article online for updates and enhancements.

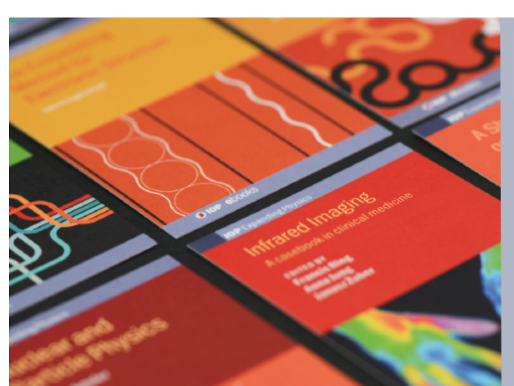

IOP ebooks™

Bringing together innovative digital publishing with leading authors from the global scientific community.

Start exploring the collection–download the first chapter of every title for free.

This content was downloaded from IP address 128.210.126.199 on 08/06/2021 at 14:40

IOP Publishing Journal of Micromechanics and Microengineering

J. Micromech. Microeng. **31** (2021) 075005 (7pp) https://doi.org/10.1088/1361-6439/ac0323

Deep isotropic chemical etching (DICE) process for fabricating highly symmetric hemispherical silicon molds

Calvin Mitchell Jones, Mustafa Mert Torunbalci and Sunil Ashok Bhave*

OxideMEMS Lab, School of Electrical and Computer Engineering, Purdue University, West Lafayette, IN, United States of America

E-mail: merttorunbalci85@gmail.com and bhave@purdue.edu

Received 16 December 2020, revised 1 May 2021
Accepted for publication 19 May 2021
Published 7 June 2021

Abstract

This paper introduces the deep isotropic chemical etching (DICE) process developed for wafer-scale manufacturing of highly symmetric hemispherical silicon molds. The DICE process uses silicon nitride concentric rings as a masking layer during hydrofluoric, nitric, acetic etching of $\langle 111 \rangle$ silicon substrate. These concentric rings pop up and widen the etch aperture as etch depth increases, thereby allowing control of vertical and lateral etch rates until reaching the desired mold dimensions. Our comparative experiments demonstrate that the pop-up rings are remarkable at creating molds with enhanced symmetry compared to the conventional pinhole masks. We have demonstrated the effectiveness of our approach compared to single pinholes by producing a super-symmetric 0.1 mm hemispherical mold ($R_Z/R_X = 1$) using two concentric rings surrounding a pinhole. We have then shown how the DICE process can be used to fabricate larger silicon molds and presented the results of a single concentric ring that achieves fabrication of a 0.25 mm-deep mold with an aspect ratio of $R_Z/R_X \approx 0.75$.

Keywords: MEMS, hemispherical resonator, hemispherical resonator gyroscope, micro/nanofabrication

(Some figures may appear in colour only in the online journal)

1. Introduction

Hemispherical shells are an essential structural part of various inertial and optical devices [1–9], and recently gaining interest in magnetic sensing systems [10, 11]. A well-known example is hemispherical resonator gyroscopes (HRGs) [3], a high-performance angular rate or rotation sensor. The HRG is made out of a structural shell that is anchored by a stem. The size and shape of the structural layer are critical for reaching optimum sensor performance where large and symmetric shells enable higher mechanical quality factor (Q), small mode-frequency split, and enhanced acceleration insensitivity [4, 12]. Northrop Grumman manufactures the most sensitive mm-scale quartz HRGs for high-speed projectiles [13]. However, these quartz gyroscopes are extremely expensive due to serial manufacturing, polishing, and assembly process. Micro-HRGs have been recently demonstrated by (a) depositing structural thin-films on pre-defined molds [12, 14–18] and (b) glass-blowing or locally blow-torching the resonator [19, 20]. These technologies are not only used for wafer-level manufacturing of HRGs, but also for various optical and magnetic sensing devices. Therefore, they evolved into 'bird-baths' [21], 'glass-blown' [22–24], 'cylinders' [17], 'whispering gallery-mode [7, 25]', and 'pierced-shell' [26] resonators.

The pre-defined mold is commonly formed by utilizing a pinhole mask on a silicon substrate and performing a type of isotropic etch using HNA (hydrofluoric, nitric, acetic) or XeF_2. However, this method has limited use due to insufficient geometry control. In the case of using a small pinhole, the etching

* Author to whom any correspondence should be addressed.

 © 2021 IOP Publishing Ltd Printed in the UK

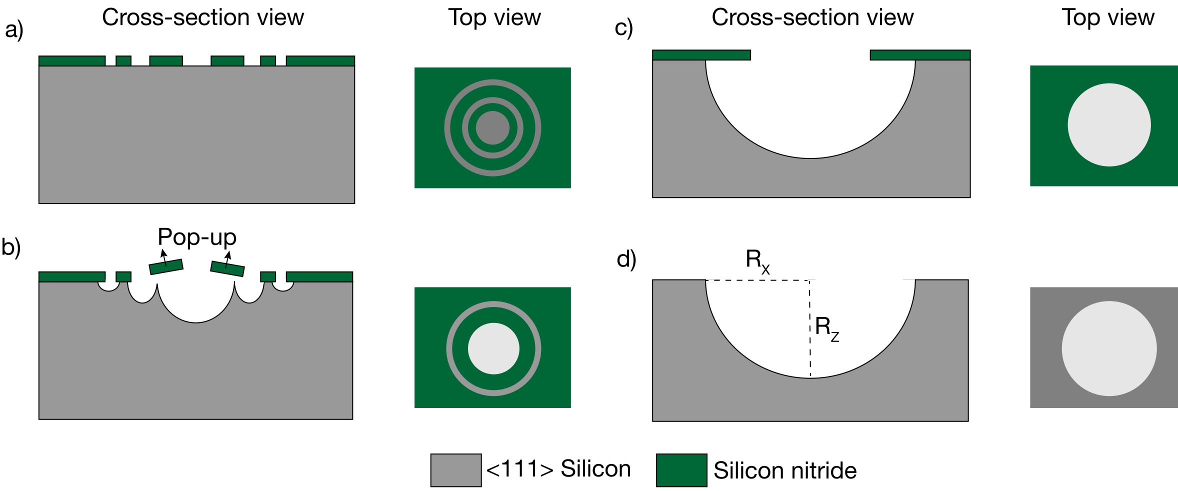

Figure 1. Main steps of the DICE process: (a) silicon nitride pop-up ring mask is patterned using a maskless aligner and etched with RIE, (b) pop-up rings fly off by etching the silicon with 1:4:1 HNA, (c) HNA etches the silicon until reaching to desired mold dimensions, (d) silicon nitride mask is stripped in hot phosphoric acid at 170°.

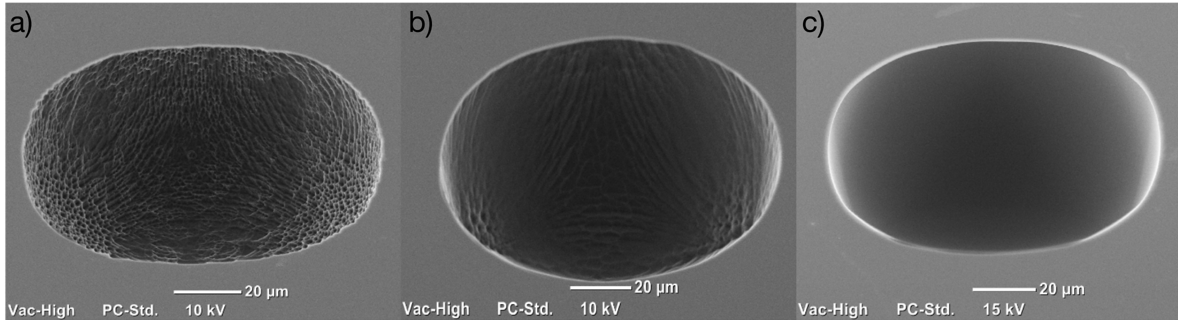

Figure 2. SEM pictures of molds etched using different HNA concentrations: (a) HNA (3:6:1), (b) HNA (1:2:1), and (c) HNA (1:4:1). The HNA concentration of 1:4:1 provides relatively faster etch rates and optimum surface roughness; thereby it is used for all experiments in the study.

process becomes diffusion-limited at a short depth. On the other hand, a large pinhole produces shallower molds as lateral dimensions become significantly larger than vertical. Alternatively, micro-glass blowing uses the combined effect of glass softening, surface tension, and internal gas pressure in order to fabricate 3D shells with very high surface quality. A similar method is blow torching that relies on the local heating and pressure difference to form very smooth 3D molds. However, both techniques have limited use since they require complex process steps and high temperatures (>1600 °C) for forming the molds. Therefore, there is a demand for a process technology that enables the manufacturing of mm-scale and highly-symmetric hemispherical molds for inertial, optical, and magnetic sensing applications. This new technology will be not only used to fabricate mm-scale, super-symmetric shells but also structural molds in any size and shape and be applicable to a wide range of materials. With a spectrum of size, shape, material possibilities, these molds become a low-cost, quick solution to the inefficiencies in current sensing applications.

In this work, we propose deep isotropic chemical etching (DICE) process that uses concentric rings around the pinhole for enhanced control of vertical and lateral etch rates. With the addition of these rings, the HNA mixture is forced into the center of the hemispherical mold first, before each ring from the center to the outside flies off and completes the hemispherical mold. In comparison to the single pinhole mask, the size of the openings and the rings can be altered in order to change the general shape and symmetry, providing excellent geometry control while maintaining the process simpler. A major benefit of the DICE process is that control of the final structure solely relies on any changes done to the ring design without major changes being needed for the actual process flow.

2. DICE process

Figure 1 presents the main steps of the DICE process. The process starts with the deposition of a 650 nm-thick silicon nitride film on a 1 mm-thick silicon substrate by using Low Pressure Chemical Vapor Deposition (LPCVD). The orientation of the silicon substrate is selected as $\langle 111 \rangle$ as in [27] in order to obtain better isotropic etching properties. The pop-up rings are patterned by spinning an AZ1518 photoresist on the silicon nitride film and then performing contactless exposure with a 405 nm wavelength using the Heidelberg maskless

Table 1. Summary of different masking structures and related design variations used throughout the paper.

Experiment	Design	Pinhole (μm)	Ring-1 (μm)	Ring-2 (μm)	Gap-1 (μm)	Gap-2 (μm)	Design variation
(A) Pinhole & gaps	1	10–50	—	—	—	—	Pinhole
	2	10–50	6	8	4	2	Pinhole with fixed rings and gaps
	3	10–260	6	8	4–30	2	Pinhole + Gap-1
	4	50–260	6	8	4–30	2–15	Pinhole + Gap-1 + Gap-2
(B) Rings & gaps	5	80–260	12–60	16–80	12–30	2	Pinhole + Ring1 + Ring2 + Gap1
	6	80–260	12–60	—	12-30	—	Pinhole + Ring1 + Gap1 (Single ring)

aligner. The silicon nitride film is etched by using a CHF_3 and O_2 gas mixture with Reactive Ion Etching (RIE) (figure 1(a)). An isotropic wet etch using HNA is performed to produce the silicon mold. Figure 2 compares different HNA concentrations in terms of surface roughness. The HNA concentration is selected as 1:4:1 for enabling relatively faster etch rates and smooth mold surfaces. The pop-up rings allow for HNA to perform a deep isotropic etch for the center of the mold first before popping off the inside ring, with an exothermic reaction (figure 1(b)). The etch is then completed by popping off the outside ring to create the symmetrical hemispherical mold (figure 1(c)). All HNA etches are performed at room temperature with chips laying flat and face up. The etching is done until approximately 150 nm of the silicon nitride mask is left (approximately for 90 min) in order to maintain the integrity of the mold while maximizing etch depth. The silicon nitride mask is finally removed in hot phosphoric acid (figure 1(d)) at 170 °C for 30 min. The mold dimensions and mask integrity are monitored using an SEM and a surface profilometer.

3. Design of experiments and results

We performed two sets of experiments in order to fabricate mm-scale hemispherical silicon molds with an aspect ratio close to 1. The target aspect ratio of 1 is determined based on [12] in which a perfect hemisphere is shown to achieve enhanced acceleration insensitivity. Table 1 summarizes different masking structures such as a single pinhole, a pinhole surrounded by a single ring, and a pinhole with two concentric rings and related design variations used throughout the paper. Figure 3 illustrates the cross-section and top view of a pop-up ring design that consists of a center pinhole surrounded by two concentric rings. For all experiments, we used completely identical process conditions and methodology in order to make a precise comparison. The aspect ratio is calculated by dividing vertical etch depth (R_Z) to lateral etch depth (R_X).

The first experiment includes four different structural designs for testing the vertical etch limits by incrementally varying the dimensions of pinhole and gaps. Figure 4 presents the fabrication results of Design-1 and Design-2. For Design-1, a smaller single pinhole creates a symmetric but only smaller molds (up to 70 μm). We observed that the etch rate

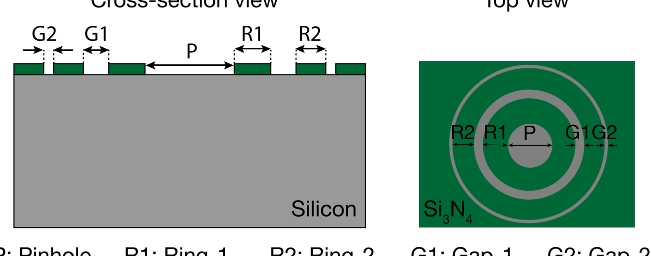

Figure 3. Cross-section and top views of pop-up rings. The main design parameters are the dimensions of the pinhole (P), rings (Ring-1 and Ring-2), and gaps (Gap-1 and Gap-2).

becomes significantly slower after a certain depth. Due to diffusion limitation, HNA etch has a tendency to etch horizontally rather than vertically, causing a shallow mold. There is a limited etch time that can occur before HNA completely consumes the silicon nitride mask. Similarly, a larger pinhole results in shallower molds since the initial etch window is very large. Design-2 relatively solves the issue of single pinholes by allowing for more controlled openings spread across a larger area that allow for the deeper etch before the mask is completely consumed by HNA. However, after a certain limit, Design-2 shares similar characteristics to Design-1. This is because by only opening up the center pinhole, the area that is being etched is not able to increase and the etch is still being focused in the center limiting it to similar sizes. These results show that Design-1 is a satisfying option for symmetric molds up to 70 μm and Design-2 is a good candidate for 100 μm deep symmetric molds. However, these designs are not useful for larger hemispheres (>100 μm) since they both become diffusion-limited after a certain depth.

In order to further scale these designs, the pinhole, gap-1, and gap-2 are increased in a controlled way. In Design-3, the pinhole is increased 10 to 260 μm in almost 30 μm increments while also increasing the inner gap-1. On the other hand, Design-4 includes similar structures but this time gap-2 is also increased. Figure 5 presents the fabrication results of Design-3 and Design-4. These results show that scaling is not linear by just increasing the pinhole and gap dimensions and the vertical etch depth is limited at around 150 μm for these structures. The exothermic reaction that allows the pop-up rings to fly off and create a hemispheric mold depends

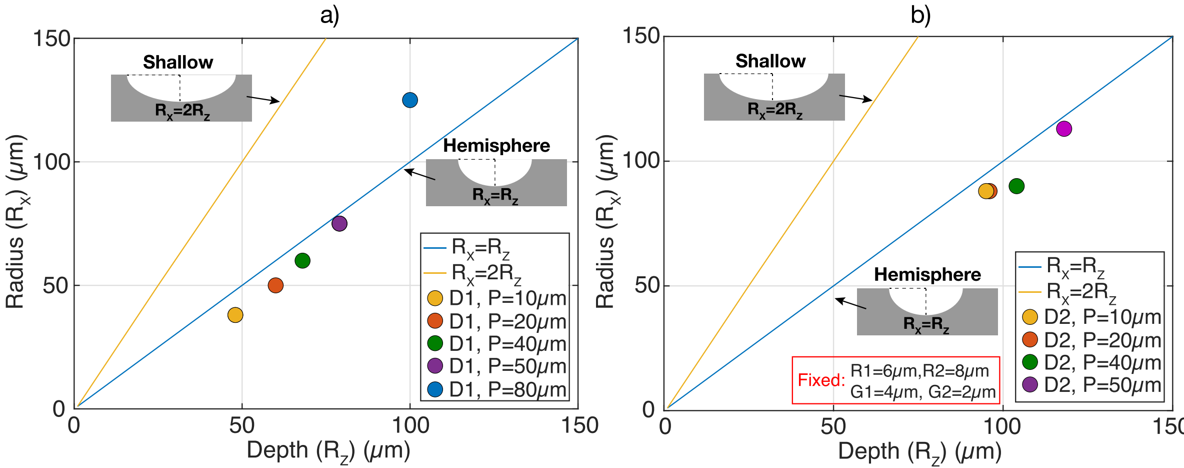

Figure 4. Fabrication results of Design-1 and Design-2: (a) Design-1 (only pinhole) is excellent for fabricating highly symmetric but only smaller hemispherical molds up to $\approx$ 70 μm. However, when the initial pinhole opening increases (D1, P = 80 μm), the final mold becomes shallower. (b) Design-2 (a pinhole with two concentric rings) can achieve an excellent symmetry for larger devices (up to $\approx$ 100 μm) but after a while, it behaves like a single pinhole and gets diffusion-limited.

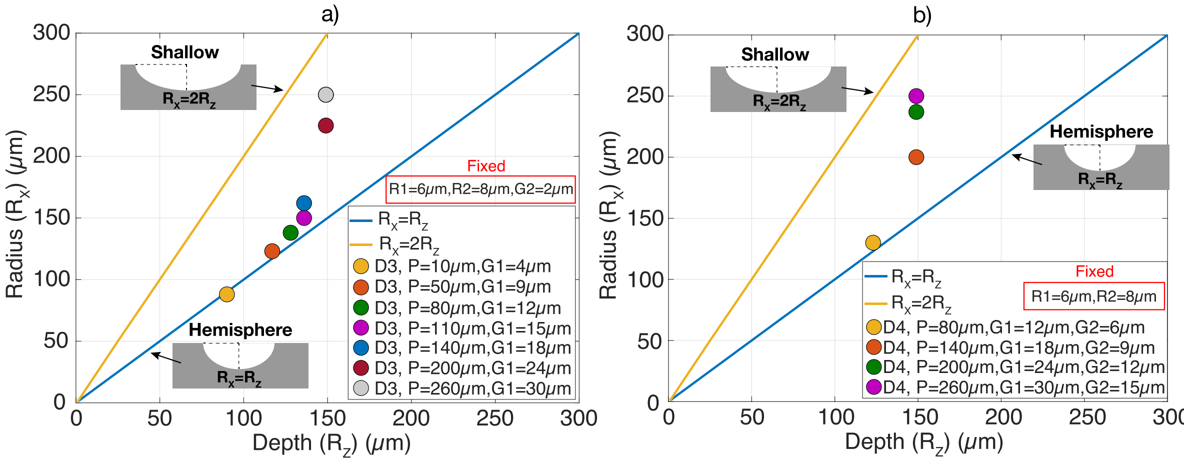

Figure 5. Fabrication results of Design-3 and Design-4: (a) in Design-3, pinhole, and gap-1 are incrementally increased. This approach works well until the mold dimensions reach a depth of 150 μm. The mold does not scale linearly as we increase the pinhole and gap-1 more. (b) In Design-4, pinhole, gap-1, and gap-2 are incrementally increased. It is observed that increasing the gap-2 results in larger R_X and the final mold became very shallow.

on how much HNA is allowed into the mold. Designs 3–4 have shown that openings become much larger since the rings flew off too quickly. The fly-off time can be reduced by increasing the width of the silicon nitride rings. This way, a longer vertical etch can be done before the rings fly off. Therefore, in the second experiment, we investigated the effect of ring width and different ring combinations on the mold symmetry. In Design-5, the width of two concentric rings, pinhole, and gap-1 are incrementally increased while keeping the gap-2 fixed. We also compared the number of pop-up rings for achieving the best aspect ratio. Therefore, in Design-6, the width of a single ring and pinhole is swept while keeping the gap-1 the same. Figure 6 compares the fabrication results of Design-5 and Design-6. It is observed that Design-6 presents larger molds that have more symmetric hemispherical shapes. Design-5 is shown to create larger molds with deeper etches, but the aspect ratio trends more toward shallower structures. Moreover, Design-6 includes only a single ring, simplifying the design variations and control. Overall, Design-5 may allow different shapes for different applications but will be limited or difficult to manage when trying to create larger, highly symmetric hemispheric molds. In comparison, the Design-6 provides an enhanced design control due to the design's ability to create larger more symmetric molds with greater ease than the two ring design. Figure 7 compares the cross-section SEM pictures as well as surface profilometer measurements of shallow and hemispherical silicon molds fabricated using Design-5 and Design-6. The cross-section SEM images are taken using control samples that are simultaneously etched with the main samples. These control chips are then cleaved and etch profiles are relatively compared. The cross-section SEM images demonstrate that Design-6 achieves a more hemispherical etch profile. On the other hand, the radius of the mold (R_X) is measured by taking a top-view SEM of the main sample. The main

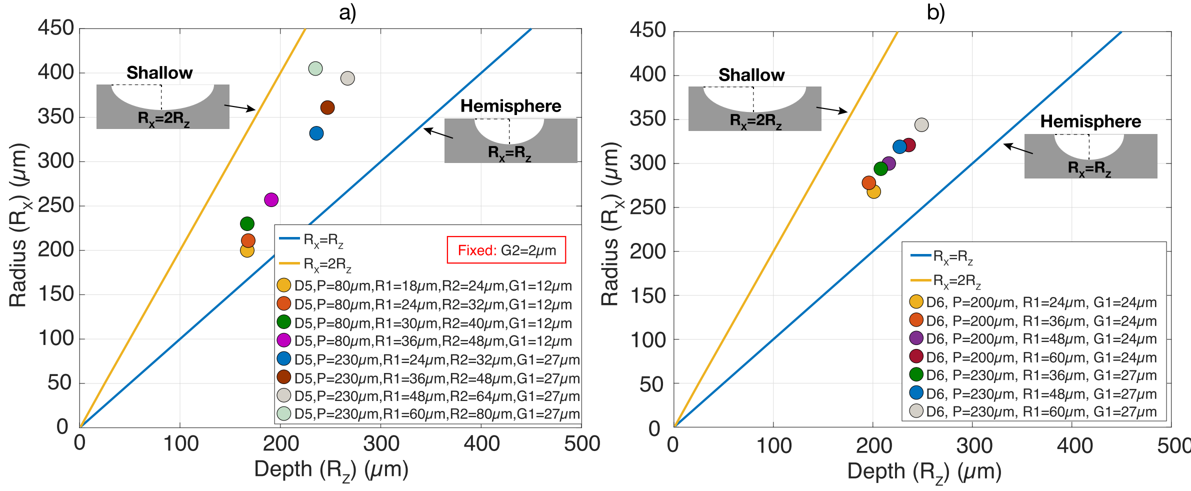

Figure 6. Fabrication results of Design-5 and Design-6: (a) in Design-5, the width of two concentric rings, pinhole, and gap-1 are incrementally increased while keeping the gap-2 fixed, (b) in Design-6, the width of a single ring and pinhole are swept while keeping the gap the same. A single pop-up ring gives the symmetry of 0.73 for a wide range of dimensions.

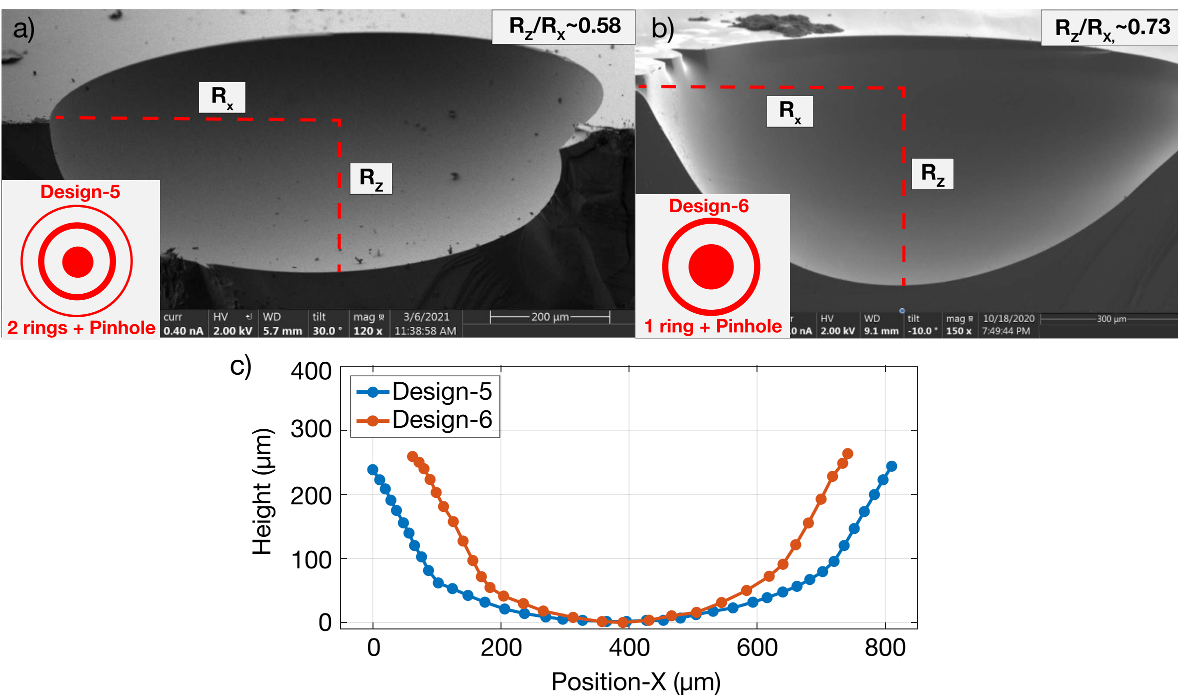

Figure 7. SEM pictures of (a) shallow and (b) hemispherical silicon molds fabricated using different ring designs, (c) surface profilometer measurements of Design-5 and Design-6. Design-6, a single ring with a pinhole, achieves fabrication of a 0.25 mm-deep silicon mold with an aspect ratio of 0.73 whereas it is 0.58 for Design-5, two concentric rings with a pinhole, resulting in a shallower mold.

samples are also used to measure the etch depth (R_Z) with a surface profilometer. It is hard to accurately measure the steep periphery region with the existing surface profilometer. Therefore, the slope region is not used as a parameter for the comparison. A single ring with a pinhole achieves fabrication of a 0.25 mm-deep silicon mold with an aspect ratio of 0.73 whereas it is 0.58 for two concentric rings with a pinhole, producing a shallower mold.

In summary, it is found that Design-1 is practical for applications that require hemispherical structures smaller than 70 μm. These structures would be too small for optimum device operation for inertial sensing applications. For the initial proof-of-concept, Design-2 is created to show the effectiveness of concentric rings to fabricate larger hemispheric structures while having more control over the aspect ratio. An aspect ratio ($R_Z/R_X = 1$) of 1 is achieved for structures around 100 μm but severely degrades as the design reaches beyond 150 μm. With Designs 4–5, we have observed that a larger ring width is needed to prevent the rings fly off so quickly for balancing vertical and lateral etch rates for deeper etches. After implementing the wider rings, a deeper etch is achieved with Design-5, but the amount of design factors involved makes it

difficult to control the aspect ratio as the etch becomes deeper. Therefore, Design-6 has become the optimum solution to the issues found in the other types of designs. This single ring surrounding a pinhole is not only able to create a deeper etch (0.25 mm) while maintaining the aspect ratio close to 1 but also reduces the number of design factors that are difficult to control as the structure grows larger.

4. Conclusions

We have proposed the DICE process, a novel method for wafer-level fabrication of highly symmetric silicon molds. This unique process uses concentric pop-up rings to enable precise control of vertical and lateral etch rates in silicon etching with HNA. We have experimentally shown that the DICE process is much better at creating molds with balanced symmetry and size compared to the conventional approaches. Another key advantage of the DICE process is its flexibility: different pop-up designs can produce molds with the desired shape, dimensions, or roughness by using appropriate process conditions. Furthermore, the method can be applied to various materials and etchants for different applications. The geometry control can be improved by implementing predictive modeling. This will make even deeper etches with a better aspect ratio possible. We believe that the DICE process is a powerful platform with its simplicity and flexibility and may become a unique solution to the fabrication inefficiencies in inertial, optical, and magnetic sensing applications.

Data availability statement

All data that support the findings of this study are included within the article (and any supplementary files). The data that support the plots within this paper and other findings of this study are available on Zenodo (www.zenodo.org)

Acknowledgment

The authors would like to acknowledge Dr Noah Opondo, Hao Tian, and Ozan Erturk of the OxideMEMS lab at Purdue University for assistance with SEM imaging and valuable discussions on the process flow.

ORCID iDs

Mustafa Mert Torunbalci https://orcid.org/0000-0001-9625-669X
Sunil Ashok Bhave https://orcid.org/0000-0001-7193-2241

References

[1] Hashimoto H, Tanaka S and Sato K 1991 Silicon acoustic lens for scanning acoustic microscope (SAM) *TRANSDUCERS'91* pp 853–9

[2] Albero J, Nieradko L, Gorecki C, Heidi Ottevaere V Thienpont G, H, Pietarinen J, Päivänranta B and Passilly N 2009 Fabrication of spherical microlenses by a combination of isotropic wet etching of silicon and molding techniques *Opt. Express* **17** 6283–92

[3] Rozelle D M 2009 The hemispherical resonator gyro: from wineglass to the planets *Proc. 19th AAS/AIAA Space Flight Mechanics Meeting* vol 134 pp 1157–78

[4] Senkal D and Shkel A M 2020 *Whole Angle MEMS Gyroscopes: Challenges and Opportunities* (New York: Wiley)

[5] Bhat A K, Fegely L C and Bhave S A 2014 GOBLIT: a giant opto-mechanical bulk machined light transducer *Hilton Head 2014* pp 247–50

[6] Fei C *et al* 2017 Ultrahigh frequency ZnO silicon lens ultrasonic transducer for cell-size microparticle manipulation *J. Alloys Compd.* **729** 556–62

[7] Zhang C, Cocking A, Freeman E, Liu Z and Tadigadapa S 2017 On-chip glass microspherical shell whispering gallery mode resonators *Sci. Rep.* **7** 1–11

[8] Sumaria V and Tadigadapa S 2020 Whispering-gallery-mode optical microshell resonator infrared detector *IEEE Sens. J.* **21** 2634–41

[9] Hu Y, Yang H, Wang T, Mao X, Xie R, Liang J, Qin G, Wang M and Long G 2020 A novel method to fabricate on-chip ultra-high-Q microtoroid resonators *Opt. Commun.* **476** 126259

[10] Freeman E, Wang C-Y, Sumaria V, Schiff S J, Liu Z and Tadigadapa S 2018 Chip-scale high q-factor glassblown microspherical shells for magnetic sensing *AIP Adv.* **8** 065214

[11] Xia J, Qiao Q and Zhou G 2020 Controllable gap in microsphere resonator integrated with a deformable ferrofluid droplet for magnetic field sensing *Opt. Fiber Technol.* **58** 102292

[12] Torunbalci M M, Dai S, Bhat A and Bhave S A 2018 Acceleration insensitive hemispherical shell resonators using pop-up rings *2018 IEEE Micro Electro Mechanical Systems (MEMS)* (IEEE) pp 956–9

[13] Trusov A *et al* 2016 mHRG: miniature CVG with beyond navigation grade performance and real time self-calibration *2016 IEEE Int. Symp. on Inertial Sensors and Systems* (IEEE) pp 29–32

[14] Bernstein J J, Bancu M G, Cook E H, Chaparala M V, Teynor W and Weinberg M S 2013 A MEMS diamond hemispherical resonator *J. Micromech. Microeng.* **23** 125007

[15] Sorenson L, Gao X and Ayazi F 2012 3-D micromachined hemispherical shell resonators with integrated capacitive transducers *2012 IEEE 25th Int. Conf. on Micro Electro Mechanical Systems (MEMS)* (IEEE) pp 168–71

[16] Heidari A *et al* 2013 Micromachined polycrystalline diamond hemispherical shell resonators *2013 Transducers & Eurosensors XXVII: The 17th Int. Conf. on Solid-State Sensors, Actuators and Microsystems (Transducers & Eurosensors XXVII)* (IEEE) pp 2415–18

[17] Saito D, Yang C, Heidari A, Najar H, Lin L and Horsley D A 2015 Batch-fabricated high q-factor microcrystalline diamond cylindrical resonator *2015 28th IEEE Int. Conf. on Micro Electro Mechanical Systems (MEMS)* (IEEE) pp 801–4

[18] Bai Z, Wang Y, Zhao Q, Yang Z, Cui J and Yan G 2019 Improved HNA isotropic etching for large-scale highly symmetric toroidal silicon molds with <10-nm roughness *J. Micro-Nanolithogr. MEMS MOEMS* **18** 044501

[19] Cho J Y, Yan J, Gregory J A, Eberhart H W, Peterson R L and Najafi K 2013 3-dimensional blow torch-molding of fused silica microstructures *J. Microelectromech. Syst.* **22** 1276–84

[20] Zotov S A, Trusov A A and Shkel A M 2012 Three-dimensional spherical shell resonator gyroscope

fabricated using wafer-scale glassblowing *J. Microelectromech. Syst.* **21** 509–10

[21] Cho J Y, Woo J-K, Yan J, Peterson R L and Najafi K 2013 Fused-silica micro birdbath resonator gyroscope (μ-BRG) *J. Microelectromech. Syst.* **23** 66–77

[22] Senkal D, Ahamed M, Trusov A A and Shkel A M 2013 High temperature micro-glassblowing process demonstrated on fused quartz and ULE TSG *Sens. Actuators* A **201** 525–31

[23] Senkal D, Ahamed M J, Ardakani M H A, Askari S and Shkel A M 2014 Demonstration of 1 million *Q*-factor on microglassblown wineglass resonators with out-of-plane electrostatic transduction *J. Microelectromech. Syst.* **24** 29–37

[24] Wang R, Bai B, Feng H, Ren Z, Cao H, Xue C, Zhang B and Liu J 2016 Design and fabrication of micro hemispheric shell resonator with annular electrodes *Sensors* **16** 1991

[25] Zhang C, Cocking A, Freeman E, Liu Z and Tadigadapa S 2017 Whispering gallery mode based on-chip glass microbubble resonator for thermal sensing *2017 19th Int. Conf. on Solid-State Sensors, Actuators and Microsystems (Transducers)* (IEEE) pp 630–3

[26] Hamelin B, Tavassoli V and Ayazi F 2017 Microscale pierced shallow shell resonators: a test vehicle to study surface loss *2017 IEEE 30th Int. Conf. on Micro Electro Mechanical Systems (MEMS)* (IEEE) pp 1134–7

[27] Fegely L C, Hutchison D N and Bhave S A 2011 Isotropic etching of 111 SCS for wafer-scale manufacturing of perfectly hemispherical silicon molds *2011 16th Int. Solid-State Sensors, Actuators and Microsystems Conf.* (IEEE) pp 2295–8